Multidisciplinary Journal of Geology and Earth Sciences
Volume 11 Issue 2, April-June 2023
ISSN: 2995-3669
Impact Factor: 7.76
http://kloverjournals.org/journals/index.php/ges

FRIGID FORMULAS: DECIPHERING WINTER MINIMUM TEMPERATURE VARIATIONS IN YIXING THROUGH COMPARATIVE RESEARCH

Yifan Jiang, Chun Mei Wu
Yixing Meteorological Bureau, Yixing, Jiangsu, 214206, China
Wuxi Meteorological Bureau, Wuxi, Jiangsu, 214135, China

Abstract: Yixing, situated in the southwestern region of Jiangsu province, displays marked variations in winter minimum temperatures due to its intricate topographical and landscape features. Given the backdrop of global climate shifts and the increasing frequency of extreme weather events, there arises an imperative to advance predictive technologies for meteorological disasters characterized by extremely low temperatures. As urbanization, rapid economic growth, population expansion, and the progress of facility agriculture surge ahead, areas at high risk for low-temperature phenomena like rain, snow, and ice have migrated from northwest to southeast China. While the overall risk of low temperatures in southern China is declining, the potential for major disasters has surged in recent times. Prior studies have laid a robust theoretical foundation for bolstering the monitoring and diagnosis of extreme low-temperature weather events. These studies also provide critical insights into the distinctive features of winter low temperatures in Yixing. Nevertheless, these endeavors often encompass spatial scales too extensive to be directly applicable to the Yixing region, where notable local microclimatic discrepancies frequently arise. This study endeavors to leverage station data specific to the Yixing area, conducting a comprehensive analysis of winter minimum temperatures across the county. The aim is to elucidate the fundamental causes of these variances, ultimately refining the forecasting of low-temperature events

Keywords: Yixing, winter minimum temperatures, extreme low-temperature events, meteorological disasters, local microclimates.

1. Introduction

Yixing, located in the southwestern tip of Jiangsu province, exhibits notable variations in winter minimum temperatures due to its complex topography and landscape. Given the context of global climate change and the frequent occurrence of extreme weather and climate events [1-3], there is a growing necessity to enhance the research on forecasting technologies for extreme low-temperature meteorological disasters. As urbanization, rapid economic development, population growth, and the advancement of facility agriculture accelerate, the regions at high risk of low-temperature rain, snow, and ice have shifted from the northwest to the southeast of China [4]. Although the risk of low temperatures in southern China has a downward trend, the possibility of major disasters has increased in recent years [5,6]. The aforementioned studies lay a solid theoretical foundation for improving the

monitoring and diagnosis of extreme low-temperature weather and climate events, as well as offering research insights into exploring the characteristics of winter low temperatures in Yixing. However, these studies often encompass spatial scales that are too large to be directly applied to the Yixing region, where significant regional differences in local microclimates are frequently observed [7-10]. In this study, we aim to utilize the station data available in the Yixing region to analyze winter minimum temperatures throughout the county, elucidate the underlying causes of these differences, and thereby refine low-temperature forecasting.

2. EOF decomposition

After adjusting the winter daily minimum temperatures of 26 stations in the Yixing area from 2015 to 2020 to the same altitude as the national station, an EOF decomposition was conducted on their monthly anomalies. The resulting patterns were subjected to a North significance test. The typical errors of the first three EOF modes were 19.08, 0.22, and 0.12, respectively. The corresponding eigenvalues for the first three modes were 57.26, 0.65, and 0.33, respectively. Additionally, the variance contributions of the first three eigenvectors were 97.53%, 1.11%, and 0.56%, respectively. Notably, the typical error ranges of the first two eigenvalues do not overlap and exhibit distinct separation. These two modes collectively account for a cumulative contribution rate exceeding 98%. These findings suggest that the first two eigenvectors effectively characterize the two distributions of the monthly mean minimum temperature during the winter from 2015 to 2020.

The EOF1 mode exhibits a significantly higher variance contribution compared to the other modes, representing the primary spatial distribution pattern of the monthly temperature field in Yixing city during winter (Figure. 1). The eigenvalues of the EOF modes are all negative, indicating a consistent overall warming trend in the monthly mean minimum temperature across all stations in Yixing during the study period. The region with lower values is situated in the hilly southwest area of Yixing, suggesting greater variability in monthly minimum temperatures in that specific area compared to other parts of Yixing. This observation aligns with the geological heat capacity around the stations: the eastern area along Taihu Lake and the densely networked water bodies possess higher geological heat capacity and exhibit a relatively weaker warming trend, whereas the southwestern region and the M5856 station, characterized by hilly terrain, have lower geological heat capacity and demonstrate a stronger warming trend.

Multidisciplinary Journal of Geology and Earth Sciences
Volume 11 Issue 2, April-June 2023
ISSN: 2995-3669
Impact Factor: 7.76
http://kloverjournals.org/journals/index.php/ges

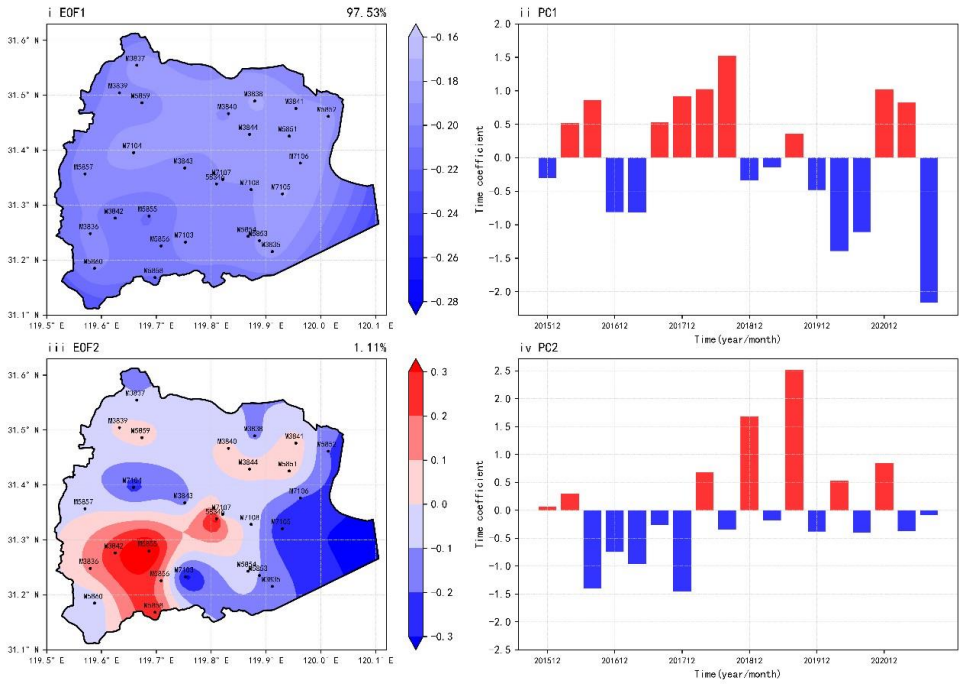

Figure 1 EOF decomposition of the monthly mean minimum temperature anomaly in winter from 2015 to 2020

The EOF2 mode represents a combination of positive and negative values, with 58346 and the southwest hilly region situated in the higher positive value range. The center of negative values is located on both sides of the positive center region. When considering the time coefficient, in the early period, there is a decreasing trend with predominantly negative values. During this time, the minimum temperature in the central and southwestern parts is significantly lower than the surrounding areas. In the middle and late period, positive and negative values are mixed, with noticeably higher positive values and an overall upward trend. When the positive values are prominent, the minimum temperature in the central and southwestern parts is significantly higher than the surrounding regions. Notably, even though stations 58346, M7107, M5856, and M7103 are adjacent and share comparable geological conditions, they still exhibit certain differences, which will be further investigated in the subsequent analysis.

3. Adjacent station difference

The average difference between the minimum temperatures at station 58346 and station M7107 during the winter period of 2015-2020 was -1.95℃, with a median of -1.9℃ and a standard deviation of 1.59℃. There were 542d where the temperatures at both stations were the same or station 58346 was higher by only 16d, accounting for 2.95% of the total days, with a maximum deviation of 0.3℃. The maximum deviation below the average was 5.4℃, and the majority of the days (49d) had temperatures below the average by 0.2℃, accounting for 9.04% of the total days. Regarding the difference interval performance, which is established by $\mu \mp \sigma$ (hereafter referred to as σ), there were 157d and 144d falling within the $\mp\sigma$ interval, accounting for 29.0% and 26.6% respectively. Additionally, there were 102d and 130d falling

Multidisciplinary Journal of Geology and Earth Sciences
Volume 11 Issue 2, April-June 2023
ISSN: 2995-3669
Impact Factor: 7.76
http://kloverjournals.org/journals/index.php/ges

within the ∓2σ interval, accounting for 18.8% and 24.0% respectively. And there were 130d falling within the -3σ interval, accounting for 1.7%

3.1 Circulation situation

Synthetic analysis was performed by the day of the occurrence of the difference interval, the previous day and the two previous days, and anomaly analysis was performed with the average field of the 30-year whole winter period from 1990 to 2010, respectively.

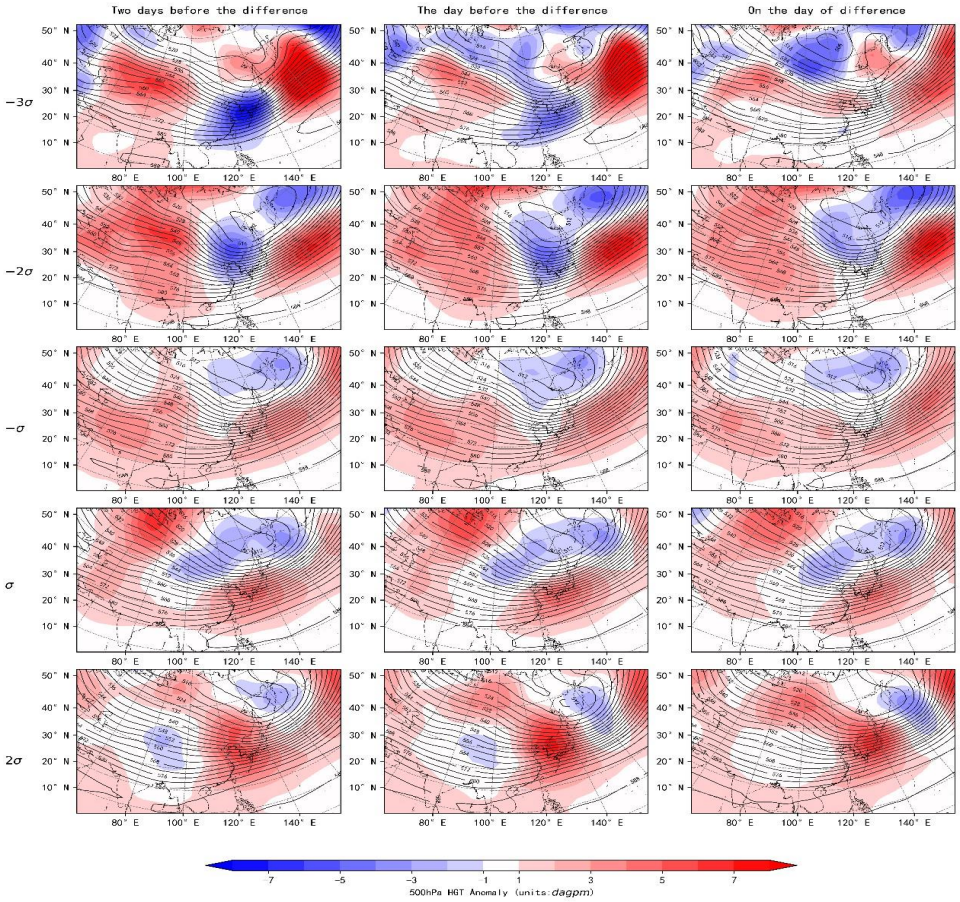

Figure 2 Synthetic analysis of the 500hPa geopotential height of each interval (contours are the synthetic mean field of the interval, shading is the anomaly, units: dagpm)

In the 500hPa geopotential height situation field (Figure 2), the -3σ interval corresponds to the passage of a deep low-pressure trough. Two days prior to its occurrence, the middle and high latitudes exhibit a ridge-trough-ridge pattern. The Ural ridge area is stronger than usual for winter, and the East Asian trough is unusually intense. The trough extends to the two regions, while the middle latitudes are dominated by northwest airflow behind the trough. In the Yixing area, the transit of cold air is more intense than during a typical winter. However, the overall cold air in the -2σ region is relatively weaker and slightly delayed in its time phase. Initially, the Yixing area experiences the influence of westward airflow at the bottom of the trough, transitioning to the control of northwest airflow behind the trough on the same day. During the first two days of the -σ interval, the cold air in East Siberia is slightly

stronger than usual, while the Yixing area experiences weaker cold air due to the influence of westward airflow. In the σ interval, the middle and high latitudes exhibit a ridge and two troughs pattern. There is an unusually strong high-pressure ridge in winter, extending from Novaya Zemlya to the Caspian Sea. The intensity of the short-wave trough disaggregated from Siberia is stronger compared to the -σ interval. In the Yixing area, the warm and humid airflow is stronger due to the influence of southwesterly airflow ahead of the splitting trough. In the 2σ interval, both the ridge and trough systems are weaker than in the σ interval. The middle and low latitudes are affected by the eastward development of the deeper south branch system, leading to three days of stronger warm and humid airflow in the Yixing area.

In the 700hPa wind field (Figure. 3), within the -3σ interval, the winds in the middle and high latitudes west of Novaya Zemlya and south of Iceland converge towards the critical area of the cold wave (where wind speeds are significantly stronger than in a typical winter). From there, the winds strongly move southward along the northwest path, resulting in stronger-than-normal winter winds from the west side of Lake Baikal to the northern part of Jiangsu Province. In the Yixing area, the wind speed experiences variations over a three-day period: initially weakened, then significantly weakened. In the -2σ and -σ intervals, the cold air from the middle and high latitudes in the -3σ interval divides into two streams. The -2σ interval corresponds to the cold air east of Novaya Zemlya along the northwest path via the critical area of the cold wave, while the -σ interval corresponds to the cold air south of Iceland along the same path. During the -σ interval, the Yixing area is influenced by westerly airflow for three days, and its wind speed does not significantly deviate from that of a normal winter.

Within the σ interval, the wind speed of the southwest airflow is slightly stronger than in a typical winter, particularly on that specific day. Within the 2σ interval, the south branch system in the middle and low latitudes is strong, leading to significantly stronger southwest winds in the two regions compared to a normal winter. The Yixing area is affected by this strong southwesterly airflow.

Multidisciplinary Journal of Geology and Earth Sciences
Volume 11 Issue 2, April-June 2023
ISSN: 2995-3669
Impact Factor: 7.76
http://kloverjournals.org/journals/index.php/ges

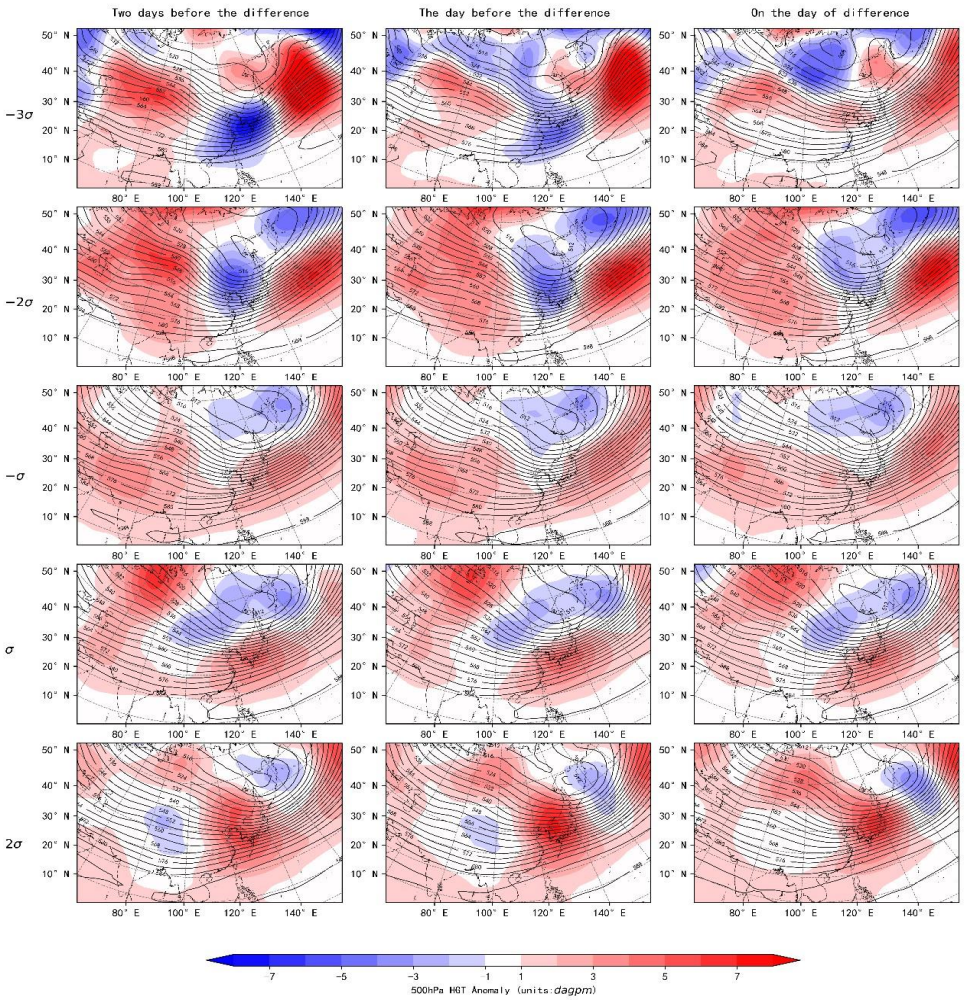

Figure 3 Synthetic analysis of wind field at 700hPa in each interval (wind scale is the synthetic mean field in the interval, shading is the anomaly, unites: m/s)

3.2 Peripheral topography

A synthetic time series analysis was conducted for the nine processes within the -3σ difference interval (Figure 4). From the isobaric vertical profile, there was evident northwest airflow with vertical cold advection from the early low level to the upper level. The vertical velocity was > 0.15Pa/s in the middle and low levels. Near the ground level, the airflow gradually shifted to southerly at 22:00 on the previous day. However, when the temperature difference occurred, there was still noticeable vertical cold advection in the middle and lower layers, with a vertical velocity of 0.15Pa/s maintained between 950 and 800hPa. The maximum wind speed at 10m above the ground did not exceed 3 m/s at the two stations during this period, and it was even lower than 1 m/s during low temperature periods. Regarding the terrain, when considering the wind direction as the center, the average height difference between the terrain within a semicircular area from 12.5 to 187.5m, 200 to 587.5m, and 600 to 1000m downwind distance within 180° of the station and the height of the station was determined. Station 58346 was

Multidisciplinary Journal of Geology and Earth Sciences
Volume 11 Issue 2, April-June 2023
ISSN: 2995-3669
Impact Factor: 7.76
http://kloverjournals.org/journals/index.php/ges

slightly lower or close to the terrain in the near distance, while the terrain upwind and downwind in the middle distance was 5m higher than the station, and nearly 10m higher in the long distance. On the other hand, station M7107 was higher and relatively flat in the short distance, but 5m lower than the station in the long distance. Due to the topography and terrain, it was easier for cold air downwind of the lower terrain in station 58346 to accumulate, which affected the temperature at the measurement station. The wind speed at 10m was lower at station M7107, but it was higher than the surrounding terrain. Therefore, even with evident vertical cold advection, the cold air could disperse in the vicinity, and accumulation was less likely. As the cold air accumulated around station 58346, the temperature difference between the two stations increased from 2.7℃ at 06:00 of the previous day to 4.3℃ at 07:00 of the same day. Subsequently, the low level gradually shifted to southerly airflow, and the ground wind also turned southerly. Station 58346 was downwind of lower terrain, but the terrain at a middle distance was still 5m higher. Coupled with the low wind speed at the ground level, even after 07:00 on the following day, the two stations still had a temperature difference of 2.6℃.

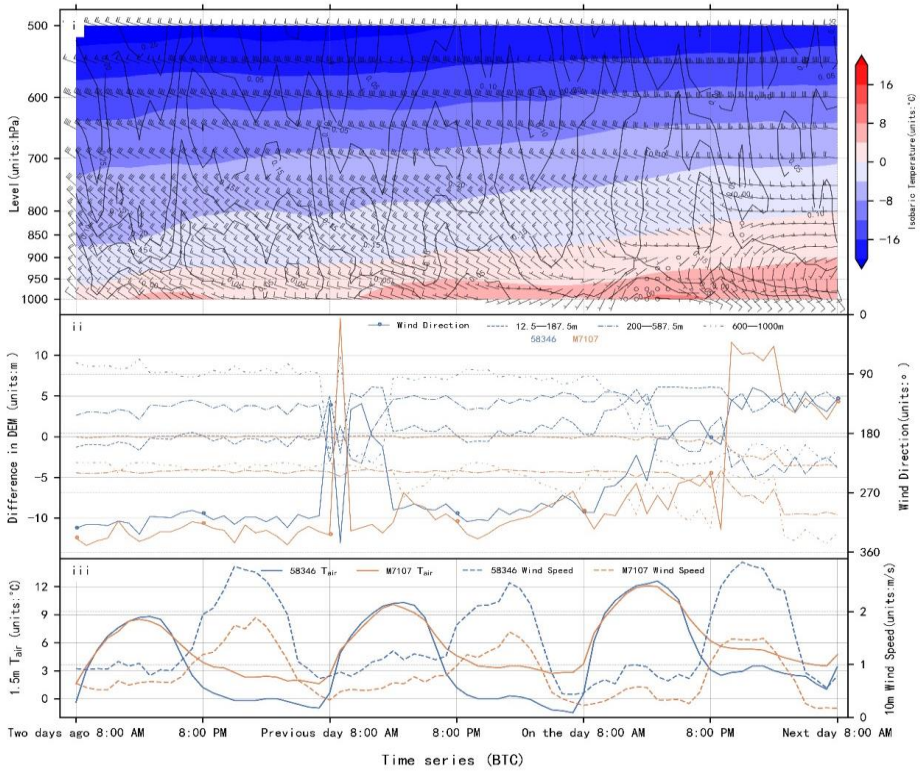

Figure 4 -3σ interval meteorological key time sequence diagram (i shading: isobaric surface air temperature (℃), wind plume: isobaric surface wind speed (m/s), contour: isobaric surface vertical velocity (Pa/s); ii two stations whole point wind angle (°) and downwind direction and station terrain height difference (m); iii two stations whole point 1.5m air temperature (℃) and 10m wind speed (m/s)) The topographic differences between M5856 and M7103 are more obvious: M5856 and M7103 have hilly uplands with southwest to north direction between the two stations, and M7103 is on the

leeward slope of winter wind while M5856 is on the upwind direction of windward slope. The topography around the two stations also has obvious differences on the degree of cold air accumulation. Therefore, the overall spatial distribution of the minimum temperature in the Yixing area can be characterized as follows: when influenced by southwesterly airflow, the overall difference in minimum temperature in the Yixing area is not significant. However, under clear sky conditions, areas with high heat capacity geology around the measuring station will exhibit relatively higher minimum temperatures, while areas with low heat capacity geology will show lower minimum temperatures. In areas with similar geological conditions, terrains that are more conducive to the accumulation of cold air will experience significantly lower minimum temperatures. Based on the aforementioned findings, we will proceed to validate the results using a deep learning model, focusing on station 58346.

4. Model Validation

A feedforward neural network was constructed using the PyTorch framework, consisting of a single hidden layer with 128 neurons and a sigmoid activation function. The model utilized mean square error (MSE) as the loss function and employed the Adam optimizer for updating model parameters and selecting the optimal model through a callback function. The training set encompassed the winter period from 2015 to 2020, while the forecast set covered the winter of 2021.For Model1, the eigenvalues were selected to incorporate various data sources, including Era5 reanalysis data from the preceding two days, historical anomalies, real-time observational data, and forecast data from 20:00 to 08:00. Model2 excluded cloud data from the forecast, Model3 removed wind direction and speed data, and Model4 incorporated a topography-based judgment of the cold air accumulation effect (assigning a value of 0 to the height difference exceeding the wind speed within a 1km downwind direction of 180° from the station, and 1 otherwise).

The accuracy of each model, with an error tolerance of within 1°C, was 70.0%, 55.6%, 65.6%, and 76.7% for Model1, Model2, Model3, and Model4, respectively (Figure 5). Model 2 exhibited a significant decrease in accuracy and demonstrated an inverse relationship with Model 1 during certain time periods, suggesting that sky conditions had a notable impact on the minimum temperature around areas with low heat capacity geology. After excluding wind data in Model 3, some influence remained, but the overall trend of change remained relatively consistent. Model 4 showcased an improvement in accuracy, with its change trend aligning more closely with the actual values.

Multidisciplinary Journal of Geology and Earth Sciences
Volume 11 Issue 2, April-June 2023
ISSN: 2995-3669
Impact Factor: 7.76
http://kloverjournals.org/journals/index.php/ges

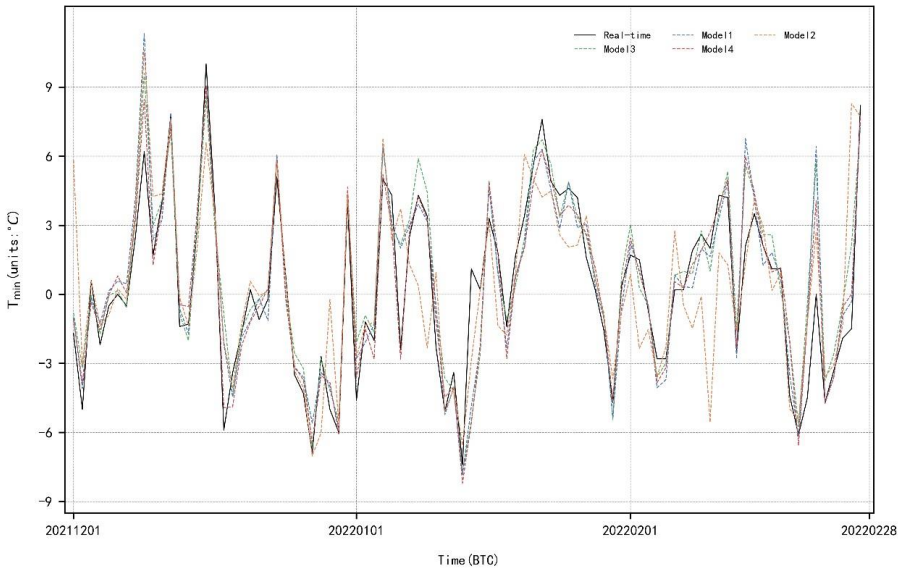

Figure 5 Predicted results of minimum temperature with different eigenvalues (units: °C)

Therefore, adding the judgment of cold air accumulation effect to the forecast of winter minimum temperature can help improve its accuracy.

5. Conclusion

The overall monthly average temperature in the Yixing area during the winter period from 2015 to 2020 exhibits an increasing trend. The increase is relatively weaker in the eastern part, near Taihu Lake and the dense water network area, while the southwestern hilly area with low geological heat capacity experiences a more pronounced temperature rise.

When the sky is cloudy, the overall difference in minimum temperature across the Yixing area is not significant. However, under clear sky conditions, stations situated in areas with low geological heat capacity display lower minimum temperatures. This effect is particularly evident in stations that are conducive to the accumulation of cold air.

By incorporating topographical considerations into the feed forward neural network model developed using the PyTorch framework, the accuracy of minimum temperature forecasting can be significantly improved. This model effectively takes into account the impact of topography on the accumulation of cold air.

Data Source

2015-2020 winter surface minimum temperature observations in Yixing, ERA5 reanalysis data, NASA DEM HGT topographic data.

Acknowledgement

Funding: This paper was supported by Wuxi Meteorological Research Fund (K202203).

References

Brabson B B, Palutikof J P. The evolution of extreme temperatures in the central england temperature record: the evolution of extreme temperatures [J]. Geophysical Research Letters, 2002, 29(24): 16-1-16–4. DOI:10.1029/2002GL015964.

Li W, Li Y, Chen L, et al. Inter-decadal variability of the relationship between winter temperature in china and its impact factors [J]. Journal of Applied Meteorological Science, 2013, 24(4): 385–396. DOI:10.3969/j.issn.1001-7313.2013.04.001.

Bai H, Xiao D, Liu J, et al. Temporal and spatial patterns of extreme climate events and agrometeorological disasters in north china from 1965 to 2014 [J]. Geography and Geo-Information Science, 2018, 34(5): 99–105. DOI:10.3969/j.issn.1672-0504.2018.05.017.

Gao J. Analysis and assessment of the risk of snow and freezing disaster in china [J]. International Journal of Disaster Risk Reduction, 2016, 19: 334–340. DOI:10.1016/j.ijdrr.2016.09.007.

Mao S, Li D. Comprehensive assessment of low temperature, snow and freezing weather in southern china based on meteorological elements [J]. Journal of Glaciology and Geocryology, 2017, 37(1): 14–26. DOI:10.7522/j.issn.1000-0240.2015.0002.

Zong H, Bueh C, Peng J, et al. Combined disaster events of extensive and persistent low temperatures, rain/snow, and freezing in southern china: objective identification and key features [J]. Chinese Journal of Atmospheric Sciences, 2022, 46(5): 1055–1070.

DOI:10.3878/j.issn.1006-9895.2108.21052.

Peng H, Qian P, Zhu L. Local microclimate characteristics near tai lake [J]. Journal of Meteorology and Environment, 2010, 26(1): 27–31. DOI:10.3969/j.issn.1673-503X.2010.01.006.

Shao J, Li Y, Ni J. The characteristics of temperature variability with terrain, latitude and longitude in sichuan-chongqing region [J]. Journal of Geographical Sciences, 2012, 22(2): 223–244. DOI:10.1007/s11442-012-0923-4.

Castaldo V L, Pisello A L, Pigliautile I, et al. Microclimate and air quality investigation in historic hilly urban areas: experimental and numerical investigation in central italy[J]. Sustainable Cities and Society, 2017, 33: 27–44. DOI:10.1016/j.scs.2017.05.017.

Yan H, Zeng F, Dong L. Temporal and spatial variation characteristics of urban local microclimate in beijing [J]. Ecology and Environmental Sciences, 2017, 26(5): 816–823. DOI:10.16258/j.cnki.1674-5906.2017.05.012.

Multidisciplinary Journal of Geology and Earth Sciences
Volume 11 Issue 2, April-June 2023
ISSN: 2995-3669
Impact Factor: 7.76
http://kloverjournals.org/journals/index.php/ges